Seasonal patterns of CO_2 fluxes in Amazon forests: Fusion of eddy covariance data and the ORCHIDEE model

Hans Verbeeck,[1] Philippe Peylin,[2,3] Cédric Bacour,[2,4] Damien Bonal,[5,6] Kathy Steppe,[1] and Philippe Ciais[2]

Received 10 September 2010; revised 17 February 2011; accepted 23 February 2011; published 21 May 2011.

[1] In some regions of the Amazon, global biogeophysical models have difficulties in reproducing measured seasonal patterns of net ecosystem exchange (NEE) of carbon dioxide. The global process-based biosphere model Organizing Carbon and Hydrology in Dynamic Ecosystems (ORCHIDEE) used in this study showed that a standard model parameterization produces seasonal NEE patterns that are opposite in phase to the eddy flux data of the tropical evergreen forest at the Tapajós km 67 site (Brazil), like many other global models. However, we optimized several key parameters of ORCHIDEE using eddy covariance data of the Tapajós km 67 site in order to identify the driving factors of the seasonal variations in CO_2 flux in this tropical forest ecosystem. The validity of the retrieved parameter values was evaluated for two other flux tower sites in the Amazon. The different tested optimization scenarios showed that only a few parameters substantially improve the fit to NEE and latent heat data. Our results confirm that these forests have the ability to maintain high transpiration and photosynthesis during the dry season in association with a large soil depth (D_{soil} = 10 m) and a rooting system density that decreases almost linearly with depth (H_{root} = 0.1). Previous analyses of seasonal variations in eddy covariance fluxes indicated that higher GPP levels were reached in the dry season compared to the wet season. Our optimization analysis suggests that this pattern could be caused by a leaf flush at the start of the dry season increasing the photosynthetic capacity of the canopy. Nevertheless, the current model structure is not yet able to simulate such a leaf flush, and we therefore suggest improving the ORCHIDEE model by including a specific phenology module that is driven by light availability for the tropical evergreen plant functional types. In addition, our results highlight both the potential and the limitations of flux data to improve global terrestrial models. Several parameters were not identifiable, and the risk of overfitting of the model was illustrated. Nevertheless, we conclude that these models can be improved substantially by assimilating site level flux data over the tropics.

Citation: Verbeeck, H., P. Peylin, C. Bacour, D. Bonal, K. Steppe, and P. Ciais (2011), Seasonal patterns of CO_2 fluxes in Amazon forests: Fusion of eddy covariance data and the ORCHIDEE model, *J. Geophys. Res.*, *116*, G02018, doi:10.1029/2010JG001544.

1. Introduction

[2] The forest biome of Amazonia is a major component of the earth ecosystem. These forests account for 15% of global terrestrial photosynthesis [*Field et al.*, 1998] and are a major contributor to observed interannual variations in the terrestrial carbon sink [*Bousquet et al.*, 2000]. Furthermore, evaporation and condensation over Amazonia are major engines of global atmospheric circulation [*Sellers et al.*, 1997]. Unfortunately, this biome is currently facing threats from deforestation and climate change [*Malhi et al.*, 2008]. These forests are subject to increasingly severe drought episodes through the El Niño–Southern Oscillation (ENSO) [*Misra*, 2008] and possibly through deforestation-driven reductions in rainfall [*Nepstad et al.*, 2002]. The first climate projections that included dynamic vegetation and an interactive carbon cycle predicted a dieback of the Amazonian

[1]Laboratory of Plant Ecology, Department of Applied Ecology and Environmental Biology, Faculty of Bioscience Engineering, Ghent University, Ghent, Belgium.
[2]Laboratory of Climate Sciences and the Environment, Joint Unit of CEA-CNRS, Gif-sur-Yvette, France.
[3]Laboratory of Biogéochimie et Ecologie des Milieux Continentaux, Thiverval-Grignon, France.
[4]Now at NOVELTIS, Ramonville-Saint-Agne, France.
[5]INRA Kourou, UMR 745 "Ecologie des Forêts de Guyane," Kourou, French Guiana.
[6]INRA Nancy, UMR INRA-UHP 1137 "Ecologie et Ecophysiologie Forestière," Champenoux, France.

0148-0227/11/2010JG001544

forest by the year 2100 [*Cox et al.*, 2004], resulting from regional drying in Amazonia. However, the fate of the Amazonian forest predicted by global models is still highly uncertain, particularly their response and resilience to drought stress. Therefore, these models need to be thoroughly tested with observational data [*Cox et al.*, 2004].

[3] In some regions of the Amazon, global biogeophysical models have difficulties in reproducing the seasonal pattern of net ecosystem exchange (NEE) of carbon dioxide. Eddy covariance measurements of NEE of an old growth forest (Tapajós km 67 site) near Santarém (Brazil) revealed an unexpected seasonal pattern of NEE where CO_2 is lost to the atmosphere in the wet season and gained by the ecosystem in the dry season [*Saleska et al.*, 2003]. This pattern was observed at other sites in Amazonia [*Bonal et al.*, 2008] and is opposite to the standard predicted NEE seasonal cycles of several global models: TEM, IBIS [*Saleska et al.*, 2003], SiB3 [*Baker et al.*, 2008]. Two different underlying mechanisms have been proposed to explain this unexpected seasonal pattern: (1) a dominating response of respiration on precipitation patterns [*Saleska et al.*, 2003] with wetter conditions increasing respiration emissions of CO_2 and (2) a photosynthetic or phenological positive response to elevated light levels during dry season [*Huete et al.*, 2006] (i.e., leaf flush just before start of the dry season) combined with the ability to maintain high photosynthesis levels during the dry season [*Hutyra et al.*, 2007]. This ability can be sustained by deep roots which access deep soil water reserves [*Nepstad et al.*, 1994], deep soil water columns with high water storage and/or movement of water in the soil via hydraulic redistribution [*Oliveira et al.*, 2005] or capillary rise [*Romero-Saltos et al.*, 2005].

[4] *Baker et al.* [2008] could not match the SIB3 model with the NEE data of the Santarém km 83 site by including each of these effects individually. Only when the different effects were combined into the SIB3 model, the NEE followed roughly the actual unexpected observed seasonal pattern. Furthermore, *Ichii et al.* [2007] showed that rooting depth strongly controls seasonal variation in modeled Gross Primary Production (GPP) in the Amazon and that it was only when deep rooting systems (e.g., 10 m) were considered, that flux-derived or satellite-based GPP in the dry season were successfully tracked for the Tapajós km 67 site. Accordingly, *Poulter et al.* [2009] showed that deep soil water access was critical to maintain dry season GPP with the LPJmL model compared against MODIS GPP estimates, whereas implementing a seasonal LAI did not enhance simulated dry-season GPP. However, these latter authors found indications that canopy photosynthesis was also regulated by the seasonality of biochemical processes, represented by the maximum carboxylation capacity (V_{cmax}).

[5] The three mentioned studies [*Baker et al.*, 2008; *Ichii et al.*, 2007; *Poulter et al.*, 2009] are based on "manual tuning" of model parameters, or implementation of new equations encapsulating underlying processes of the observed seasonal NEE patterns. In contrast, assimilating flux tower data into land surface models with a more rigorous and statistical approach (accounting for all sources of uncertainties on model and observations) offers the opportunity to (1) constrain specific model parameter values and uncertainties, and (2) identify crucial mechanisms controlling the energy, water and carbon budgets or gain hints on missing processes in the model structure [*Williams et al.*, 2009]. This opportunity leads to improved model predictions and to a better understanding of the underlying processes of observed patterns.

[6] In this study we optimized the parameters of a process-based model using eddy covariance data of the Tapajós km 67 site (Brazil) in order to mimic the seasonal response of CO_2 and water fluxes to dry/wet conditions in this tropical forest ecosystem. We validated the optimized model at two different flux tower sites in the Amazon: Reserva Jaru (Brazil) and Guyaflux (French Guiana). We used the Organizing Carbon and Hydrology in Dynamic Ecosystems (ORCHIDEE) global model that describes water, energy and CO_2 flux variations driven by climate, vegetation and soil information, as well as biomass, litter and soil carbon pools dynamics [*Krinner et al.*, 2005]. ORCHIDEE is the land surface component of an earth system model used for the next IPCC climate simulations. By optimizing the model parameter values, we tried to identify the driving factors of the seasonal CO_2 flux response in the Amazon. We use a Bayesian method that allows to account for prior knowledge on the parameters and to fully account for different sources of uncertainties. We tested whether the ORCHIDEE model is able to simulate the correct seasonal cycle of fluxes in response to seasonal drought by optimizing several key model parameters or whether the model structure needs substantial improvements. We tried to identify the unaccounted processes by letting several parameters vary over time in the optimization (i.e., each month a new parameter value is optimized). This led to suggestions for model structure improvement. In addition, the information content of the flux data is analyzed (i.e., the ability of the data to constrain the parameters), using the posterior error covariance matrix on the parameters. We finally assessed the relevance of the optimization by comparing the optimized parameters to available field data.

[7] More precisely, the following questions are addressed: (1) What is the potential of NEE and latent heat (LE) measurements from a single flux tower site to optimize the parameters of a process-based terrestrial model ORCHIDEE? (2) Does the model calibration at one site improve the simulation at other similar sites in the Amazon basin? (3) Which of the previous mentioned mechanisms (respiration or photosynthesis/phenology) is dominating the seasonal NEE pattern at the Tapajós site? (4) What are the unaccounted processed that need to be included in ORCHIDEE for improved simulations for evergreen tropical forest ecosystems?

2. Materials and Methods

2.1. Site Description

[8] The Tapajós National Forest km 67 site (54°48′ W, 2° 51′ S) is described in detail by *Saleska et al.* [2003]; a brief description is given here. The Tapajós National Forest is located on the eastern side of the Tapajós river, and extends from 50 to 150 km south of the city of Santarém, Para, Brazil. The study site is an old-growth moist tropical evergreen forest, but it is likely that the site is recovering from recent disturbance that created high mortality (possibly triggered by drought associated with strong El Niño events of the 1990s) resulting in a small net sink or even a source of

Table 1. General Information on the Flux Tower Sites Used for Optimization (Tapajós) and Validation (Reserva Jaru and Guyaflux)

	Tapajós	Reserva Jaru	Guyaflux
Country	Brazil	Brazil	French Guiana
Period	2002–2004	2000–2002	2004–2006
Latitude; longitude	2.85°S; 54.80°W	10.08°S; 61.93°W	5.28°N; 52.91°W
Canopy height	40–55 m	35–45 m	35 m
Altitude	88 m	191 m	35 m
Dry season	Jul–Nov	May–Sep	Sep–Dec
Flux data reference	*Saleska et al.* [2003]	*von Randow et al.* [2004] and *Kruijt et al.* [2004]	*Bonal et al.* [2008]

CO_2 because the woody biomass is currently growing and the soil is probably losing carbon. The average annual temperature and humidity are 25°C and 85%. Soils are nutrient-poor clay oxisols with low organic content. Observations in deep soil pits near the site found roots up to 12 m depth [*Nepstad et al.*, 2002]. The canopy is characterized by large emergent trees up to 55 m height and a closed canopy at about 40 m. The average annual precipitation is 1920 mm yr^{-1}, with typically a 5 month dry season between July and November (months with less than 100 mm of rainfall). During El Niño years much of the Amazon basin experiences decreased precipitation with large spatial and inter annual variation [*Misra*, 2008]. There are relatively strong seasonal variations in solar radiation, air temperature, and vapor pressure deficit which all increase substantially with the seasonal decline in precipitation, while soil moisture declines.

[9] The validity of the model parameters retrieved for the Tapajós site was further tested for two other sites in Amazonia, the Guyaflux which is located in French Guiana and also encounters strong seasonal variations in environmental conditions [*Bonal et al.*, 2008] and the Reserva Jaru site which is located in northern Rondônia, Brazil [*von Randow et al.*, 2004] (Table 1). For a detailed description of these sites, we refer to literature [*Bonal et al.*, 2008; *von Randow et al.*, 2004].

2.2. Model

[10] The ORCHIDEE biogeochemical ecosystem model (Organizing Carbon and Hydrology in Dynamic Ecosystems) was originally developed for global applications, including the coupling with atmospheric models [*Krinner et al.*, 2005]. It is a process-driven model, which calculates fluxes between the land and the atmosphere on a 30 min time step. In this study, we applied the model in "grid point mode" for individual sites, forced by 30 min gap-filled meteorological measurements from eddy covariance towers.

[11] The model contains a biophysical module dealing with photosynthesis and energy balance calculations each 30 min and a carbon dynamics module dealing with the allocation of assimilates, autotrophic respiration components, foliar development, mortality and soil organic matter decomposition on a daily time step. The standard ORCHIDEE equations are given by *Ducoudré et al.* [1993], *Krinner et al.* [2005], and *Santaren et al.* [2007]. The equations that contain the different parameters optimized in this study and the equations that differ from the mentioned publications are given in Appendix A.

[12] As in most global biogeochemical models, the vegetation is classified into plant functional types (PFT), with 13 different PFTs over the globe [*Krinner et al.*, 2005]. Distinct PFTs follow the same set of governing equations, with different parameter values for each PFT, except for the calculation of the phenology, which involves a specific functional scheme for each PFT with different equations. The considered sites were assumed to consist of one single PFT: tropical evergreen broadleaved forest, which is assumed to have no leaf seasonal cycle [*Botta et al.*, 2000]. This assumption has been adopted by many ecosystem models until recently [*Sitch et al.*, 2003; *Cox et al.*, 2004].

2.3. Data Assimilation System

[13] We optimized model parameters for the Tapajós site using a Bayesian statistical approach that accounts for all sources of uncertainties, from the model, the data and the parameters. Our approach is described in detail by *Santaren et al.* [2007] and C. Bacour et al. (Joint assimilation of eddy-covariance flux measurements and satellite observations within a process-oriented biosphere model, manuscript in preparation, 2010). With the assumption of Gaussian errors for both the observations and the prior parameters, the optimal parameter set corresponds to the minimum of the cost function $J(x)$:

$$J(x) = \frac{1}{2}\left[(y - H(x))^t R^{-1}(y - H(x)) + (x - x_b)^t P_b^{-1}(x - x_b)\right] \quad (1)$$

and contains both the mismatch between modeled and observed fluxes and the mismatch between prior and optimized parameters. x is the vector of unknown parameters, x_b the prior parameters, $H(x)$ the model and y the vector of observations. The error covariance matrices R and P_b describe the prior uncertainties on the observations and parameters, respectively. We acknowledge that the assumption of Gaussian errors might be violated for eddy covariance data [*Lasslop et al.*, 2008].

[14] To minimize the cost function we used an efficient gradient-based iterative algorithm, called L-BFGS-B [*Zhu et al.*, 1995]. This algorithm allows prescribing an upper/lower limit for each parameter. At each iteration we calculate the derivatives of $J(x)$ with the Tangent Linear model of ORCHIDEE, which was derived automatically with the numerical TAF tool (Transformation of Algorithms in FORTRAN). The L-BFGS-B algorithm does not provide uncertainties or error correlations between optimized parameters. Therefore, once the minimum is reached, the posterior error covariance matrix on the parameters P_a is calculated from the prior error covariance matrices and the Jacobian of the model at the minimum of the cost function, using the linearity assumption [*Tarantola*, 1987]. Large absolute values of the corresponding error correla-

tions (close to 1) indicate that the observations do not provide independent information to distinguish a given pair of parameters.

2.4. Eddy Flux Data

[15] Three years (2002–2004) of NEE and LE eddy covariance fluxes from the Tapajós site were assimilated for model parameter optimization. The validity of the retrieved parameters was verified for 3 years of NEE and LE data for the Jaru (2000–2002) and Guyaflux (2004–2006) sites (Table 1). The Tapajós site is the main focus of this study and its data will be described here in detail. The Tapajós site is well suited for eddy covariance measurements as it lies on exceptionally flat terrain on a plateau that extends several kilometres in all wind directions. Standard instrumentation [*Saleska et al.*, 2003] and flux data processing (correction, gap filling and partitioning) methodologies were used [*Papale et al.*, 2006; *Reichstein et al.*, 2005]. For model parameter optimization we only used original (non-gap-filled) measured fluxes of NEE and LE from 3 years of measurements (2002–2004) [*Hutyra et al.*, 2008]. Within the 3 years 47% of the half-hourly NEE and 45% of the half-hourly LE data was missing. These gaps are distributed equally over the growing season and not larger than a few days. Daily means were only calculated when more than 80% of the half-hourly data were available. The observed lack of closure of the energy balance in the eddy flux data was about 20% of the net radiation (R_n), a bias that should be kept in mind when interpreting the results for LE. Moreover, previous tests of our optimization setup [*Santaren et al.*, 2007] showed that adding sensible heat (H) and R_n to the data assimilation system did not constrain the parameters significantly better than NEE and LE alone. We therefore chose to assimilate daily mean observations of LE and NEE only.

[16] The "data" error covariance matrix (R) should include both the error on the measurements and the error on the model process representation. The random measurement error on the observed fluxes is known not to be constant [*Lasslop et al.*, 2008] and can be estimated as the residual of the gap-filling algorithm [*Moffat et al.*, 2007; *Lasslop et al.*, 2008]. On the other hand, model errors are rather difficult to assess and may be much larger than the measurement error itself. *Lasslop et al.* [2008] indicate that potential systematic errors in flux data and models would need to be addressed in data assimilation approaches. However, given the difficulties to estimate these different terms (especially the model component), we chose a simple approach, as in most previous optimization studies. The data uncertainties are defined as a function of the root mean squared error (RMSE) between the prior model and the observations (Bacour et al., manuscript in preparation, 2010). These prior errors can be further scaled in order to ensure that the final model-data misfit is consistent with the chosen uncertainties. We thus scaled the prior error for NEE by a factor of 5 in order to get similar weight in the misfit function for NEE and LE. In the results we evaluate the impact of the data error on the retrieved parameters by comparing the difference between scaling (σ_{NEE} = $RMSE_{prior}/5$) and no scaling (σ_{NEE} = $RMSE_{prior}$) for the prior NEE error. For LE, we did not scale the error (σ_{LE} = $RMSE_{prior}$), given the potential bias in energy balance closure. This resulted in uncertainties on the observed NEE and LE of 0.5 10^{-5} g C m^{-2} s^{-1} (scaled) and 20 W m^{-2}, respectively, which are comparable to the errors proposed by *Richardson et al.* [2006] and *Lasslop et al.* [2008]. These errors correspond to 5% of the maximum daytime value of each flux. The errors for NEE are of the same order of magnitude as those estimated by *Chevallier et al.* [2006] for ORCHIDEE compared to several other eddy flux tower sites.

[17] The autocorrelation and cross correlation between LE and NEE observation errors are assumed to be small in our study and are thus neglected [*Lasslop et al.*, 2008]. The model error autocorrelations, although potentially significant [*Chevallier et al.*, 2006], are also neglected in R.

2.5. Model Initialization

[18] Initial carbon pool sizes are required for each model run. Biomass and soil carbon pools are initialized to their equilibrium values from a 2000 year long spin-up driven by cycling the 3 years of climate inputs and increasing the atmospheric CO_2 concentrations from 1850 on. For Tapajós this initialization results in a modeled long-term annual NEE being a small net sink of 0.21 Mg C ha^{-1} yr^{-1}, reflecting the disequilibrium between GPP and ecosystem respiration (Reco) induced by rising CO_2. However, in reality the forest could be a net carbon sink or source depending on the time elapsed since the last disturbance. The Tapajós km 67 site was measured to be a net source of CO_2 of 1.3 Mg C ha^{-1} yr^{-1} to the atmosphere [*Saleska et al.*, 2003], attributed to a lagged response to former disturbance (see section 2.1). The quasi-equilibrium assumption used in the ORCHIDEE spin-up thus leads to errors in flux estimates [*Carvalhais et al.*, 2008]. This may disturb the retrieved parameter values and decrease the quality of the fit. Therefore optimizing vegetation and soil carbon pools at the end of the spin-up is needed for consistency with observed fluxes [*Carvalhais et al.*, 2010]. We let the inversion correct for this bias by optimizing two parameters related to the disequilibrium of carbon pools: (1) K_{soilc}, a multiplicative factor which adjusts the initial soil carbon pools from the spin-up [*Santaren et al.*, 2007], and (2) LAI_{init}, the LAI at the start of the model run correcting the LAI based on the spin-up run.

2.6. Performed Optimizations

[19] The optimized parameters and their prior values are given in Table 2. To identify the driving factors of the observed seasonal patterns in NEE and LE, we conducted several optimizations. The first optimization (O1) included only the photosynthesis parameters, the other parameters being kept constant. In each consecutive optimization we added a new group of parameters (O2–O7) (Table 3). The last optimizations (O8–O12) all included the 22 parameters of Table 2, but each of these optimizations allowed one or several parameters to vary each month. Each of the scenarios (O1–O12) was performed twice: once with unscaled errors for NEE (a-scenarios) and once with scaled errors for NEE (b-scenarios). The goodness of fit of the different optimizations was assessed by the root mean squared error (RMSE) and the Akaike information criterion (AIC) [*Akaike*, 1974]. In addition to the goodness of fit, the AIC also includes a penalty as a function of the number of estimated (optimized) parameters. This penalty discourages

Table 2. ORCHIDEE Parameters That Are Optimized in This Study and Their Prior Values for the Plant Functional Type of Tropical Evergreen Forest[a]

Parameter	Description	Prior Value	Prior Range	Units	σ_{prior}
	Photosynthesis				
V_{cmax}	Maximum carboxylation capacity	65	24–130	μmol $m^{-2}s^{-1}$	42.4
β	Ball-Berry slope	9	0–12	-	4.8
C_{Topt}	Factor controlling acclimation of optimal temperature for photosynthesis	37	17.5–48	-	12.2
C_{Tmax}	Factor controlling acclimation of maximum temperature for photosynthesis	55	27–71	-	17.6
C_{Tmin}	Factor controlling acclimation of minimum temperature for photosynthesis	2	−7 17	-	9.6
	Phenology				
LAI_{max}	Maximum obtainable LAI for a PFT	5.82	0.1–9	m^2 m^{-2}	3.56
SLA	Specific leaf area	0.0154	0.001–0.04	m^2 g^{-1}	0.0156
L_{age}	Mean critical leaf age	730	70–950	days	352
λ	Leaf clumping factor	0.63	0.5–1	-	0.2
LAI_{init}	LAI at t_0, corrected LAI from spin-up	5.82	0–9	m^2 m^{-2}	3.6
	Respiration/Carbon Balance				
Q_{10}	Temperature dependence of heterotrophic respiration	1.99372	0.5–3	-	1.0
K_{soilc}	Multiplicative factor that adjust the initial (soil) carbon stocks from spin-up	1	0.25–4	-	1.5
I_{MR}	Intercept of relation between maintenance respiration and temperature	1	0.1–2	-	0.76
S_{MR}	Slope of relation between maintenance respiration and temperature	0.12	0.001–0.5	-	0.1996
K_{GR}	Fraction of assimilates available for growth that is respired	0.28	0.1–0.5	-	0.16
	Soil Water Availability				
H_{root}	Parameter describing the exponential root profile	0.80	0.01–6.5	-	2.6
D_{soil}	Soil depth	1.5	0.1–12	m	4.76
	Stomatal Response on Soil Water Availability				
f_{stress}	Parameter that determines threshold of soil water content. Under this threshold stomata start to close.	6	0.8–25	-	9.68
	Heterotrophic Respiration Response on Soil Water Availability				
c	Parameter of soil/litter humidity function	0.29	0.1–1	-	0.36
b	Parameter of soil/litter humidity function	2.4	0.1–10	-	3.96
	Decomposition				
h_{crit}	Litter layer thickness	0.02	0.01–0.025	m	0.006
Z_{decomp}	Parameter describing the profile of organic matter content in the soil	0.2	0.05–5	-	1.98

[a]Corresponding equations are given in Appendix A. The prior errors (σ_{prior}) correspond to 40% of the prior range of variation. PFT, plant functional type.

model overfitting. We normalized both statistics according to their value for the prior model runs.

2.7. Evaluation of the Optimized Model

[20] In order to test the validity of the optimized model, the optimized set of parameters was evaluated using two independent data sets of NEE and LE from the flux towers of Guyaflux and Jaru (Table 1). The Guyaflux site is located in the very north of the neotropical rain forest, has a less strong dry season but has deep soils comparable to the Tapajós site [*Bonal et al.*, 2008]. The Jaru site is located in the southwest of Amazonia and is characterized by soils with only 3.5 m depth, where the bedrock appears [*von Randow et al.*, 2004]. The model performance for the prior and two optimized parameter sets (O7b and O11b) is evaluated for Tapajós and the two validation sites. The

Table 3. Description of the Different Optimizations Conducted in This Study[a]

Code	Description (Included Parameters From Table 2)	Number of Parameters
O1	Photosynthesis (5)	5
O2	O1 + phenology (5)	10
O3	O2 + respiration/carbon balance (5)	15
O4	O3 + soil water availability (2)	17
O5	O4 + stomatal response on soil water availability (1)	18
O6	O5 + heterotrophic respiration response on soil water availability (2)	20
O7	O6 + decomposition (2)	22
O8	O7 + monthly varying V_{cmax} (36)	57
O9	O7 + monthly varying c and b (72)	92
O10	O7 + monthly varying *SLA* (36)	57
O11	O7 + monthly varying V_{cmax}, and *SLA* (72)	92
O12	O7 + monthly varying V_{cmax}, c, b, and *SLA* (144)	162

[a]The included parameter group(s) and numbers of parameters for each optimization are given. Parameters of each group are given in Table 2. Each scenario was performed two times: (1) with unscaled errors for NEE and (2) with scaled errors for NEE.

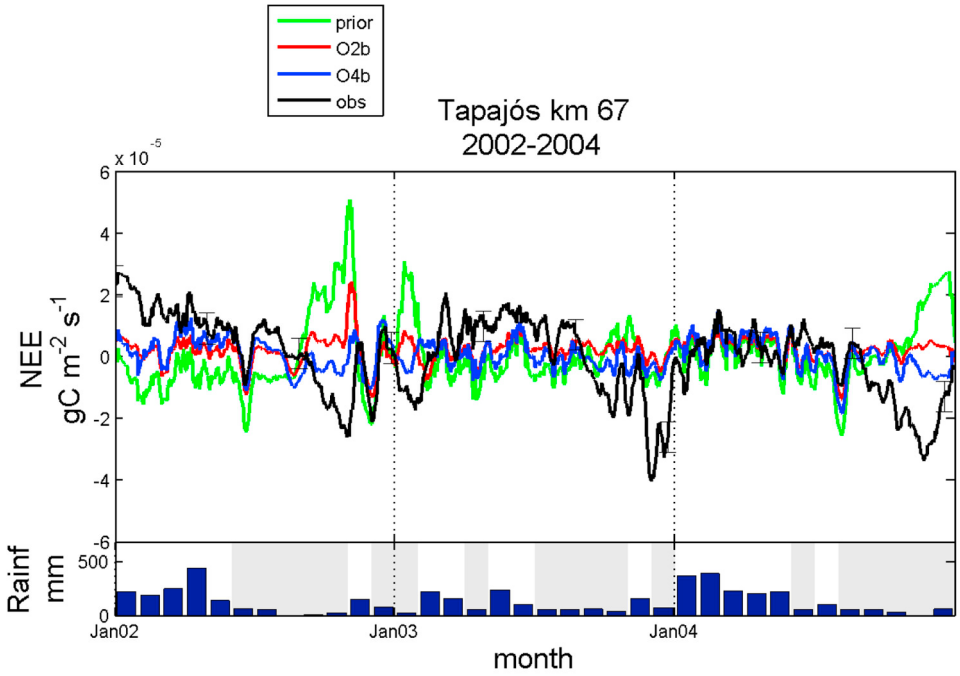

Figure 1. (top) Measured and modeled seasonal patterns of daily mean NEE (g C m^{-2} s^{-1}) of the Tapajós km 67 site (10 day running means). Eddy covariance measurements (black line) are compared with the prior model (green), optimization O2b (red), and optimization O4b (blue). (bottom) The monthly measured precipitation (mm). Dry periods are indicated in gray (<100 mm $month^{-1}$).

results are quantified using Taylor diagrams [*Taylor*, 2001]. Taylor plots are polar coordinate displays of the linear correlation coefficient (ρ), centered RMSE (pattern error without considering bias), and the standard deviation.

3. Results and Discussion

3.1. Need for Deeper Soils and Different Root Profiles

[21] In general, the prior model shows carbon uptake during the wet season (negative values of NEE) and extremely high carbon releases at the end of the dry season (Figure 1), while the measured fluxes show the opposite behavior. The only period when the prior model has a reasonable fit to the NEE data is the wet season of 2004. In contrast, the prior model generally fits nicely the LE data (Figure 2), except from a too low LE flux at the end of 2004 and a too strong decrease of LE at the end of the dry season of 2002 and 2004, showing that the model is incorrectly simulating a drought stress response at the end of the dry season. The strongest discrepancies between model and data for both NEE and LE during the dry season are found during the years 2002 and 2004.

[22] The goodness of fit of the different optimization scenarios shows that optimizing model parameters resulted in a better fit to the eddy covariance data. A general trend of the RMSE of each scenario shows that adding more parameters into the assimilation system resulted in a better model-data fit for both NEE and LE (Figure 3) (RMSE was reduced up to 50%), as expected from an increased number of degrees of freedom. The AIC value that takes into account the degrees of freedom (number of optimized parameters), indicates less improvement when more parameters are optimized. Especially for LE, overfitting is suggested as all scenarios from O5 to O12 perform equally well as O4. It is also clear that only the scenarios including the soil depth (D_{soil}) and the root profile parameter (H_{root}, describing the exponential root profile) (optimization scenarios O4–O12) were able to significantly improve the fit for both NEE and LE. This result is qualitatively similar to the results obtained by *Baker et al.* [2008] and *Poulter et al.* [2009]. Resulting seasonal flux patterns show that optimizing these two parameters (O4) is needed to remove the incorrect drought stress response from the model both for NEE (Figure 1) and LE (Figure 2).

[23] D_{soil} and H_{root} are the parameters that most significantly changed compared to their prior values in the different optimization scenarios (Figure 4). Moreover, the posterior error correlation matrix shows that the optimization is able to distinguish between these two parameters (Figure 5) (correlation is only −0.013). The resulting optimized soil depth of around 10 m (9.9 ± 3.9 m) corresponds to what is observed in the field [*Nepstad et al.*, 2002], and confirms previous modeling inferences based upon satellite greenness index values [e.g., *Kleidon and Heimann*, 1999; *Ichii et al.*, 2007] or flux measurements [*Grant et al.*, 2009]. This deep rooting pattern of Amazonian forest trees allows excess precipitation received during the wet season to be transpired during the dry season [*Nepstad et al.*, 1994] and thus provides an important mechanism to overcome seasonal drought [*Markewitz et al.*, 2010]. The resulting low value of H_{root} (0.11 ± 0.13) indicates that the vegetation is less sensitive to drought stress compared to the standard

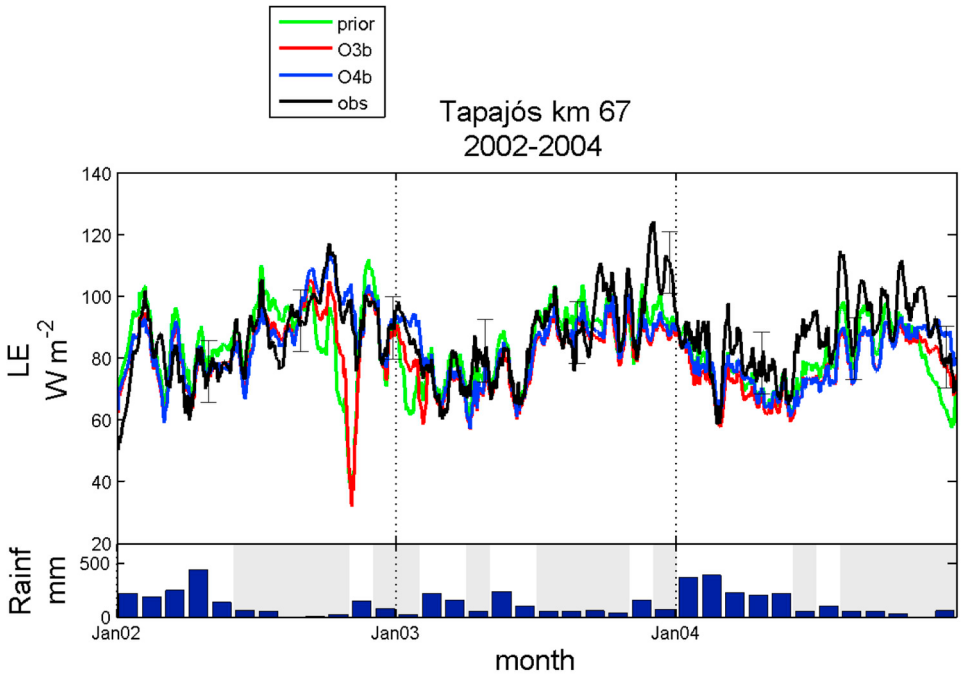

Figure 2. (top) Measured and modeled seasonal patterns of daily mean LE (W m^{-2}) of the Tapajós km 67 site (10 day running means). Eddy covariance measurements (black line) are compared with the prior model (green), optimization O3b (red), and optimization O4b (blue). (bottom) The monthly measured precipitation (mm). Dry periods are indicated in gray (<100 mm $month^{-1}$).

parameterization of this PFT (H_{root} = 0.80), because the decrease of root density with soil depth becomes less exponential and rather linear, resulting in a much slower and less strong impact of soil drying on photosynthesis and transpiration.

[24] The retrieved parameter set from scenario O7b was tested for validity at the Guyaflux and Jaru site. The Taylor plots (Figure 6) clearly indicate that the performance of the model improved substantially, both for NEE and LE, for all sites compared to the prior model performance. This confirms that the parameter set retrieved from the individual Tapajós flux site is more appropriate than the standard parameters for these tropical evergreen sites within the same region, but with different soil and climate conditions. This result highlights the potential of our approach, i.e., optimization at one site and evaluation at independent sites, to improve process-based models for a given region and ecosystem. Nevertheless, model improvement was less pronounced (i.e., the correlation coefficient did not increase) for NEE at the Jaru site. We suspect that this could be associated with the shallow soil found at this site. The validation of the parameters for different sites thus further confirms the major role of deep soils in the seasonal variations of NEE and LE in Amazonia.

3.2. Level of Constraint on the Different Parameters

[25] When comparing the different optimization scenarios using constant parameters (Figure 3, O1–O7), it appears that only a few parameters really improve the fit (soil water availability parameters, respiration parameters), while other parameters marginally contribute to a better fit (decomposition parameters, heterotrophic respiration response on soil water availability parameters, stomatal response on soil water availability). Photosynthesis and phenology parameters only improved the fit in case small errors were used for NEE (Figure 3b).

[26] From the posterior error correlations (Figure 5) it is clear that the information content of the flux data is not sufficient to distinguish between all included parameters. Nevertheless, the majority of the ORCHIDEE parameters are well constrained by the assimilated eddy covariance data, as shown by strong error reductions in Figure 4. This confirms previous studies that showed that complex models with a large amount of parameters can be well constrained by continuous eddy covariance data [*Braswell et al.*, 2005; *Santaren et al.*, 2007].

[27] The posterior error correlations give us a better insight into the structure of a complex model like ORCHIDEE. As expected, the strongest correlations (with an absolute value above 0.5) appeared between parameters of the same process (e.g., between different photosynthesis parameters or between different decomposition parameters). In addition, several interesting error correlations are found between parameters of different processes. Some of them are logical: e.g., high anti (negative) correlation between decomposition parameter c (describing the response on soil water availability) and leaf age (which is determining litter input), and the anti correlation between parameter c and the temperature dependence of the heterotrophic respiration, Q_{10}. In contrast, the anti correlation between K_{GR} (fraction of assimilates for growth that are respired) and the Ball-Berry slope β in the stomatal model is more difficult to explain (Figure 5). The

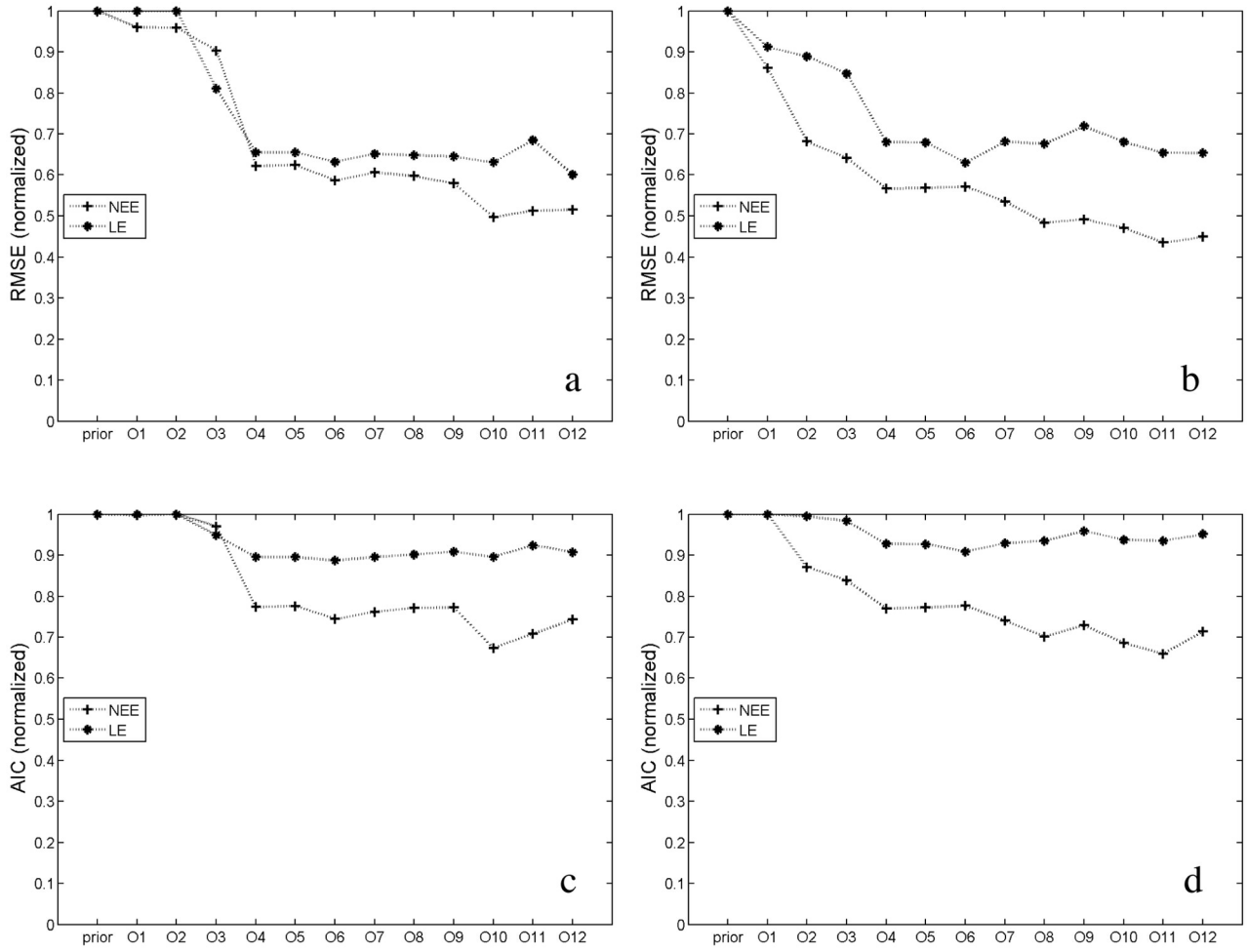

Figure 3. Goodness of fit of different optimization scenarios for NEE and LE. (a and b) Root mean squared error (RMSE) normalized against the prior RMSE for NEE and latent heat (LE) for each optimization scenario (O1–O12); (c and d) the normalized Akaike information criterion (AIC) of NEE and LE for each optimization scenario (O1–O12). Figures 3a and 3c show the results when prior errors for NEE are unscaled (σ_{NEE} = 2 10^{-5} g C m^{-2} s^{-1}); Figures 3b and 3d show results when prior errors for NEE are scaled (σ_{NEE} = 0.5 10^{-5} g C m^{-2} s^{-1}); prior errors for LE are equal in both cases (σ_{LE} = 10 W m^{-2}).

existence of large error correlations between the different ORCHIDEE parameters highlights the need for additional independent data to better constrain the model.

[28] Only small differences between posterior parameter values from the different optimization scenarios are found. It is rather difficult to compare the resulting parameters with values measured in the field. In evergreen tropical forests, there is a huge species richness and large geographical gradients in species composition [e.g., *ter Steege et al.*, 2006], which make it very difficult to obtain field measurements of parameters that are representative for the spatial scale of the flux tower footprint. Second, parameters defined from ecosystem-scale observations are different from parameters determined at the scale of the processes (i.e., leaf measurements), because of covarying effects between processes. The optimized V_{cmax} parameter (63 ± 20 μmol CO_2 m^{-2} s^{-1}) falls within the wide range of values measured at the Tapajós km 67 site (from 10 (bottom canopy) to 106 (top canopy) μmol CO_2 m^{-2} s^{-1} [*Domingues et al.*, 2005]). The resulting V_{cmax} value corresponds to values currently used in global vegetation models for tropical forests (43–82 μmol m^{-2} s^{-1} [*Domingues et al.*, 2005]), but is different from the low V_{cmax} values recently obtained by *Kattge et al.* [2009] for tropical trees on oxisols (about 29 μmol m^{-2} s^{-1}). These low values are probably an underestimation of V_{cmax} as represented in global models, because they resulted in simulations with the BETHY model [*Kattge et al.*, 2009] that underestimated the GPP of tropical forests by 21% compared to the global database of *Luyssaert et al.* [2007].

[29] The optimized values for specific leaf area SLA (0.011–0.019 m^2 g^{-1}, depending on the optimization scenario) fall within the range of the measured SLA values at the Tapajós site (0.005 m^2 g^{-1} at the top of the canopy up to 0.020 m^2 g^{-1} at the bottom of the canopy [*Domingues et al.*, 2005]).

[30] We tested all optimization scenarios with unscaled prior errors (a-scenarios) on the one hand and with scaled (5 times smaller) prior errors for NEE (b-scenarios) on the other hand, as described in the methods to investigate the influence of the weight given to the data by tightening the prior errors.

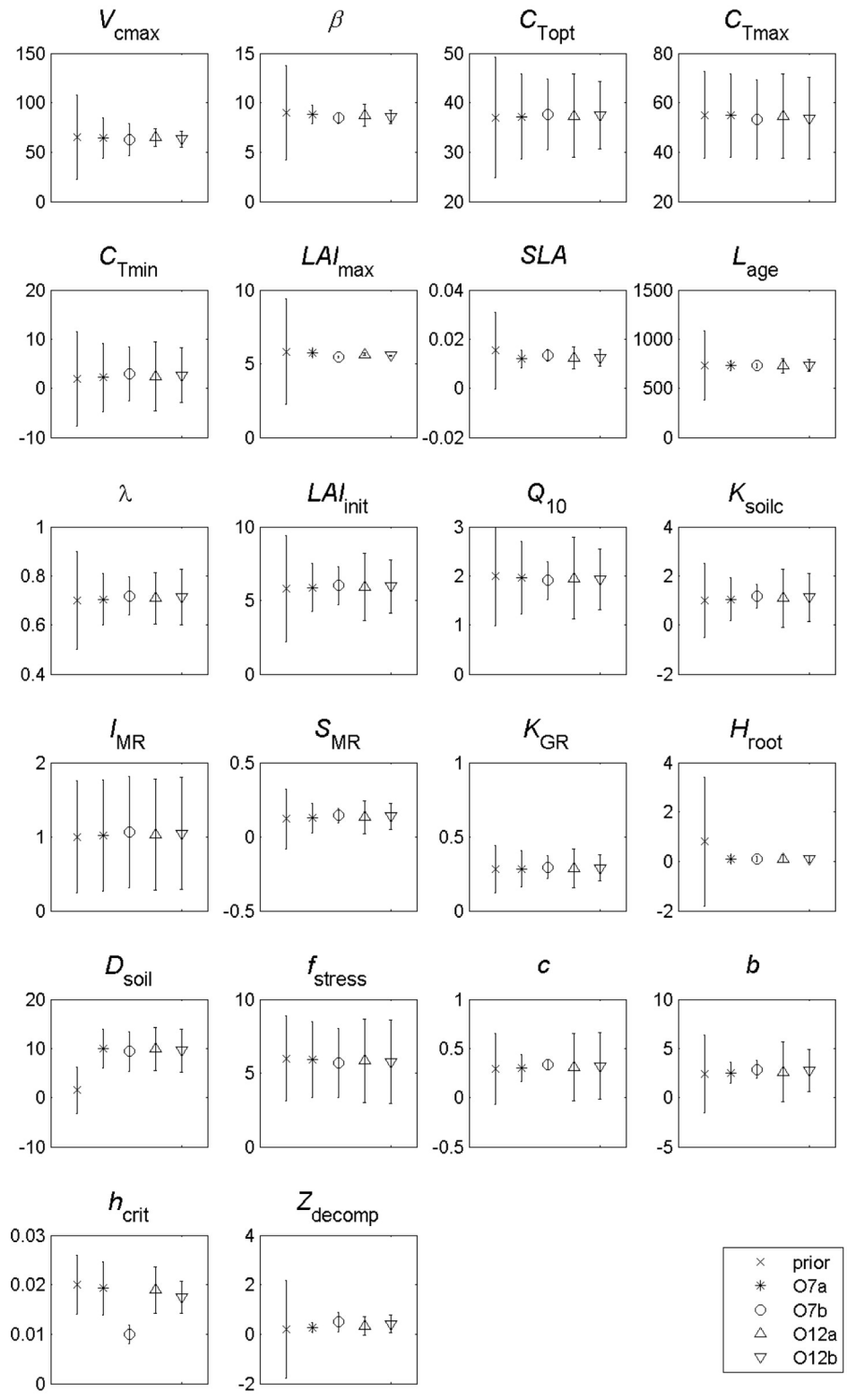

Figure 4. Resulting parameter values and their standard deviations. Prior values (crosses) are compared with optimized values: O7a (asterisks), O7b (open circles), O12a (open triangles), and O12b (open inverted triangles). Details on the optimized parameters can be found in Table 2. For the O12 scenarios: V_{cmax}, SLA, b, and c values represent means of the achieved monthly values with their standard deviations.

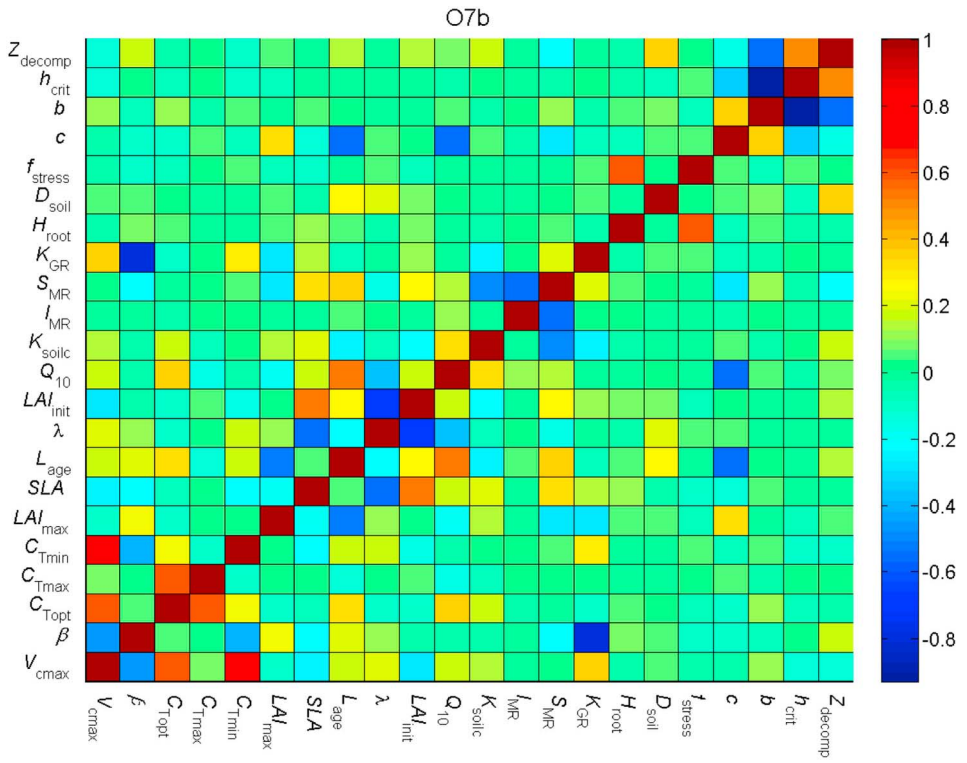

Figure 5. Posterior error correlation matrix after optimization O7b, assimilating both NEE and LE with scaled errors for NEE.

Smaller errors on NEE data increase the importance of the NEE observations in the cost function. Note that in several cases (O7–O12) this leads to a decrease of the RMSE for LE (Figure 3b). In contrast, by increasing the relative weight of NEE in the optimization, a better fit for NEE is already achieved with a few parameters only (O1–O2) (even with unrealistic soil depths of 1.5 m). As expected, the posterior error on several parameters appeared to be smaller in case of smaller errors for NEE (Figure 4). Nevertheless, the mean posterior parameter values were not significantly different in both cases.

[31] We analyzed the model-data residuals after the different optimizations and found still a strong correlation between the residuals and the magnitude of the flux (data not shown) for NEE and LE. This finding could not be explained by any significant correlation between the residuals and climatic forcing variables.

3.3. Seasonal Parameter Optimization

[32] In the different optimization scenarios O8–O12 we varied different parameters over time to investigate if they would bring more information on the underlying factors of the seasonal patterns in NEE. Although the AIC for LE (Figure 3) suggests overfitting when we compare these scenarios with the achieved fit of scenario (O7), it is clear that some extra improvement for NEE could be achieved by the different scenarios (O8–O12) (Figures 3 and 7).

[33] The resulting monthly values of the parameters b and c that describe the response of heterotrophic respiration to soil water content (Appendix A, equation (A15)) were only slightly different (lower) in the dry season compared to the wet season (data not shown). This resulted only in a marginal improvement of the fit to the NEE (O9, O12 Figure 3) and did not contribute to improve the fit to the seasonal pattern of Reco derived from eddy covariance (Figure 9b). The observed seasonality in b and c and the discrepancies between measured and modeled Reco suggest that the model structure needs a stronger response of decomposition to litter and soil humidity in evergreen tropical forests. This is in agreement with the conclusions of *Saleska et al.* [2003] on processes controlling the seasonal pattern of NEE. We anticipate that the current two layer soil hydrology model in ORCHIDEE does not provide the flexibility to define low water stress on GPP and significant water stress on heterotrophic respiration during the dry season. Therefore, the opportunity to use a multiple-layer soil hydrology [*d'Orgeval et al.*, 2008] in ORCHIDEE is promising for tropical evergreen forests.

[34] The strongest improvement of the modeled seasonal pattern of NEE was achieved by optimizing monthly values of SLA (O10) or by optimizing both SLA and V_{cmax} every month (O11, Figure 7). The resulting seasonality in these two parameters is rather weak, but both parameters show an increase during the dry season to fit the NEE and LE observations (Figure 8). The retrieved monthly parameters did not result in better model performance for the Guyaflux and Jaru site (Figure 6), showing that we cannot generalize the seasonal parameter variations inferred from one location to another. The model performance of the O11b parameter set was lower compared to the O7b parameters, which was

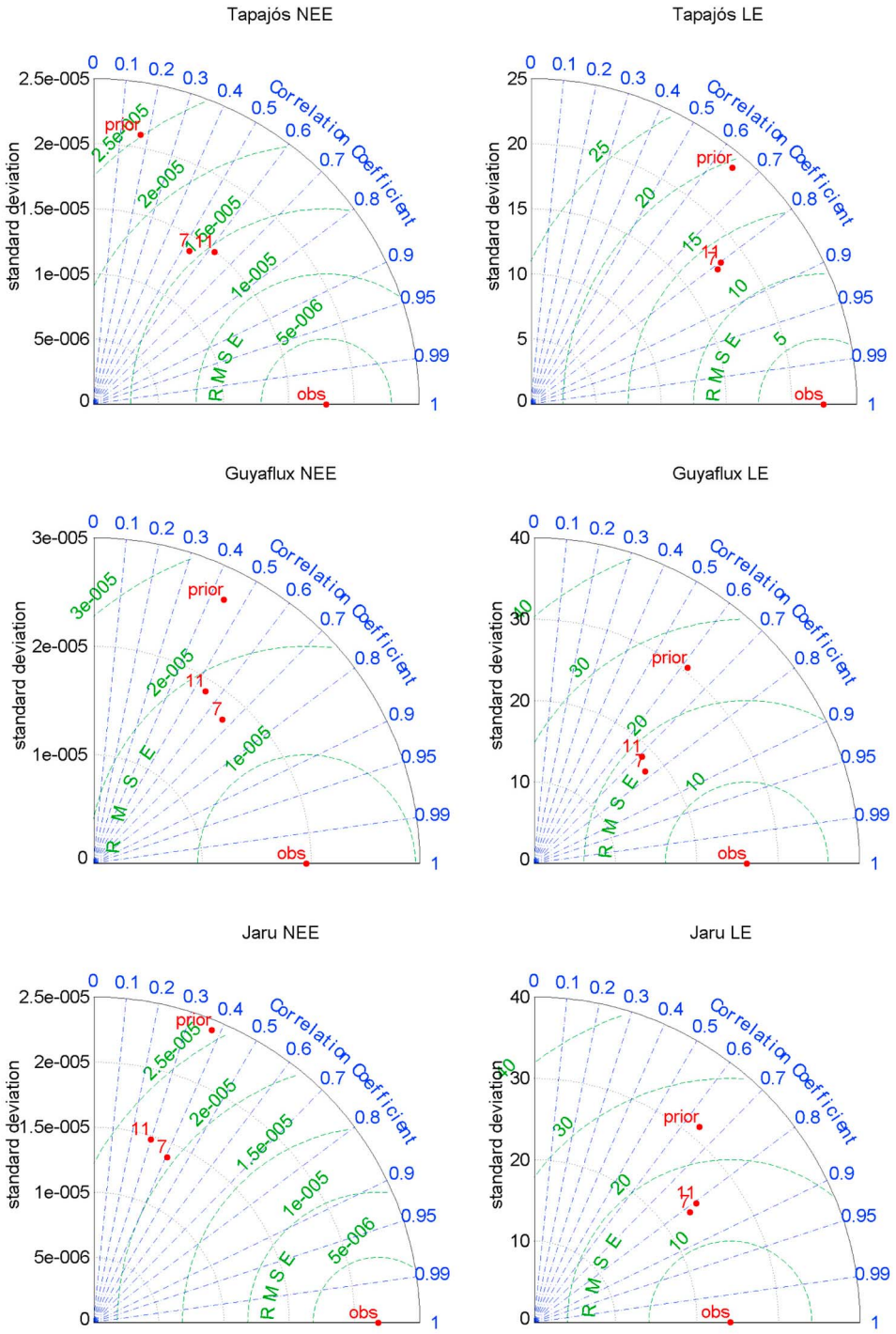

Figure 6. Taylor diagrams of model performance. The benchmark (obs) corresponds to the observed daily NEE or LE. Simulations using optimized parameter sets O7b (7) and O11b (11) retrieved at the Tapajós site are compared to the prior model (prior) performance. The model performance is shown for NEE and LE based on 3 years of daily simulated and measured values for the Tapajós, Guyaflux, and Jaru sites.

expected due to a different timing and intensity of the dry season at these locations.

[35] The seasonality observed in the parameters for Tapajós correspond qualitatively to the phenomenon of a leaf flush resulting in a weak seasonality of LAI [*Malhado et al.*, 2009] combined with an increased photosynthetic capacity during the dry season. The increased photosynthetic capacity is probably achieved by a leaf renewal at the beginning of the dry season, which is confirmed by leaf litterfall observed at the Tapajós km 67 site from July 2000

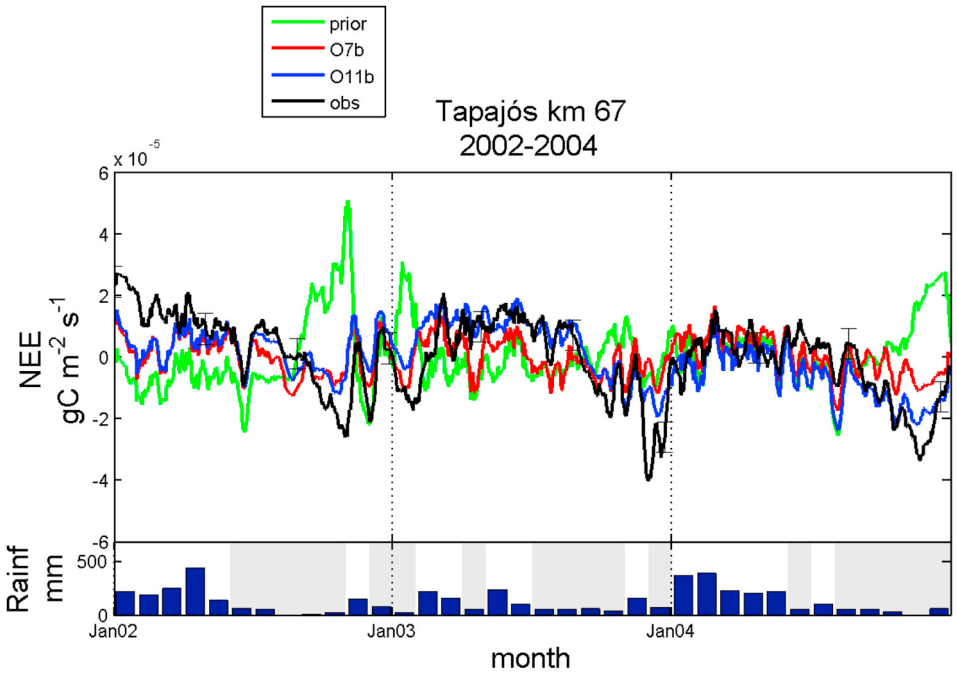

Figure 7. (top) Measured and modeled seasonal patterns of daily mean NEE (g C m^{-2} s^{-1}) of the Tapajós km 67 site (10 day running means). Eddy covariance measurements (black) are compared with the prior model (green), optimization O7b (red), and optimization O11b (blue). (bottom) The monthly measured precipitation (mm). Dry periods are indicated in gray (<100 mm $month^{-1}$).

until June 2005 [*Rice et al.*, 2008]. Leaf flush appears during the dry season when light availability is maximal and has been observed in the field at the Tapajós [*Hutyra et al.*, 2007; *Malhado et al.*, 2009] and Guyaflux site [*Bonal et al.*, 2008]. These findings confirm that solar radiation is the primary limiting factor for ecosystem processes in evergreen wet tropical forests in the Amazon, as previously suggested by modeling or remote sensing approaches [*Myneni et al.*, 2007; *Poulter et al.*, 2009].

[36] Moreover, our study highlights that the (optimized) ORCHIDEE model does not successfully simulate phenological processes for tropical evergreen forests, including the measured seasonality in leaf litterfall (not shown). To improve future versions of ORCHIDEE, we suggest including a module taking into account seasonal variations in leaf flush linked to light availability. In addition, the link of the actual V_{cmax} with leaf age in the model would synchronize the pattern of photosynthetic capacity with this leaf flush as suggested by our results.

3.4. Photosynthesis and Respiration

[37] NEE, which is relatively small in tropical evergreen forest, is the result of two large gross fluxes: photosynthesis (GPP) and ecosystem respiration (Reco). Unfortunately no direct measurements of these gross fluxes exist at stand level. However, it is interesting to compare the modeled gross fluxes with the gross fluxes derived from the NEE measurements by flux partitioning using empirical techniques.

[38] The GPP empirically derived from eddy flux measurements [*Reichstein et al.*, 2005] shows a clear seasonal pattern (Figure 9a), with high photosynthesis in the wet season and a decrease at the start of the dry season, followed by an increase of GPP during the dry season. The runs with the prior model result in seasonal patterns that strongly differ from observed values (Figure 9a). However, the unrealistic drops in GPP of the prior model at the end of the dry season disappear in the optimized model runs, and a seasonal pattern with higher GPP during the dry season is found. The optimized GPP patterns are consistent with the empirical GPP patterns observed by MODIS EVI (Enhanced Vegetation Index) [*Huete et al.*, 2006]. However, the GPP derived from eddy flux measurements show much lower values at the start of the dry season which is not consistent with both our optimized model and the MODIS EVI results [*Huete et al.*, 2006]. These inconsistencies highlight the uncertainty in all current GPP estimates during the dry season in evergreen tropical forests.

[39] A similar story appears for Reco (Figure 9b). The Reco derived values from eddy flux data after *Reichstein et al.* [2005] show a distinct seasonal pattern, with low respiration during the dry season and the highest values during wet periods. This seasonal pattern was found to dominate the resulting seasonal variations in NEE. In contrast, the optimized model shows the absence of a clear seasonal pattern, with even slightly higher respiration fluxes during the dry season. Seasonal variations in Reco in tropical rain forests strongly depend on seasonal variations in soil respiration [*Bonal et al.*, 2008]. However, soil respiration data measured with automated chambers at the Tapajós km 67 site from April 2001 to April 2003 [*Varner and Keller*, 2009] show only a slight decrease during the dry

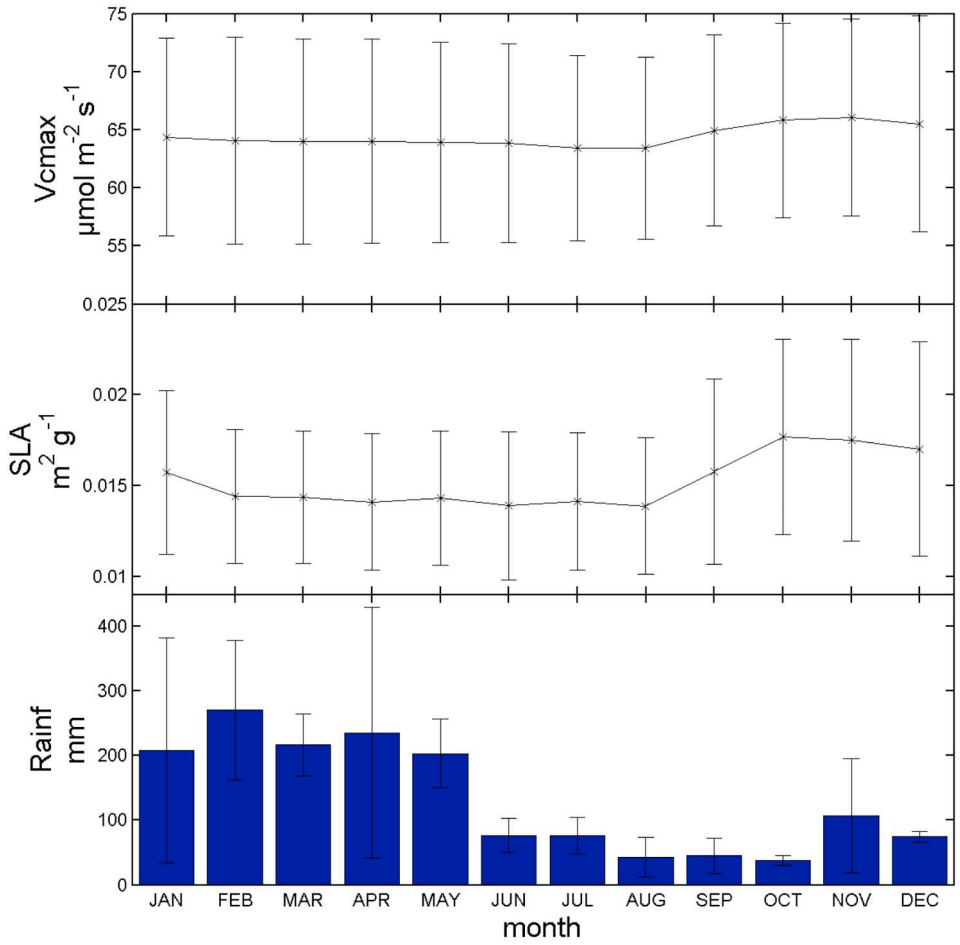

Figure 8. Mean seasonal patterns (2004–2006) of precipitation (mm) and two ORCHIDEE parameters optimized each month according to optimization scenario O11b: maximum carboxylation capacity (V_{cmax}, μmol m^{-2} s^{-1}), and specific leaf area (SLA, m^2 g^{-1}).

season (Figure 10). When we compare the seasonal pattern of modeled autotrophic and heterotrophic respiration to the measured respiration patterns (Figure 10), we must conclude that the seasonality is not well captured by the model. The simulated respiration components are probably dominated in the model by a response to temperature, which does not show a clear seasonal pattern at this site. We therefore suggest improving the respiration module with the response to soil water availability in multiple soil layers as the main driver for respiration in tropical evergreen forest.

[40] Nevertheless, the order of magnitude of the simulated heterotrophic respiration is in agreement with the soil respiration data and the ratio of the annual sum of modeled autotrophic respiration over modeled GPP (0.61) corresponds to the values for tropical forests derived from a global database ranging from 0.6 up to 0.8 [*Piao et al.*, 2010], which confirms that simulated autotrophic respiration is of the correct order of magnitude.

3.5. Carbon Pools and the Equilibrium Assumption

[41] The spin-up run to initiate the ORCHIDEE carbon pools assumes that the pools are in quasi-equilibrium, increasing steadily because GPP is driven up by increasing atmospheric CO_2. In contrast, eddy covariance and biometric observations suggest that the Tapajós km 67 site is a net source (1.3 Mg C ha^{-1} yr^{-1}) [*Saleska et al.*, 2003]. However, the biomass pools resulting from the spin-up run compare reasonably well to the observed carbon pools (Table 4). Therefore we can assume that the quasi-equilibrium assumption is appropriate to initiate the biomass pools for this study.

[42] In contrast, the total soil carbon is largely underestimated by the spin-up run (41.95 Mg C ha^{-1}) compared to the measured data from a nearby oxisol (142.1 Mg C ha^{-1}). The optimized multiplicative factor K_{soilc} increased the initial carbon pool by 20% (50.3 Mg C ha^{-1}) (Table 4). Although the initial soil carbon pool is underestimated by the spin-up run, the order of magnitude of the heterotrophic soil respiration compares well to soil respiration data, as we described in section 3.4. This apparent inconsistency is probably the result of an underestimation of the passive soil carbon pool by the ORCHIDEE modeled soil carbon dynamics based on the Century model [*Parton et al.*, 1988]. Sensitivity tests that increased the passive soil carbon pool

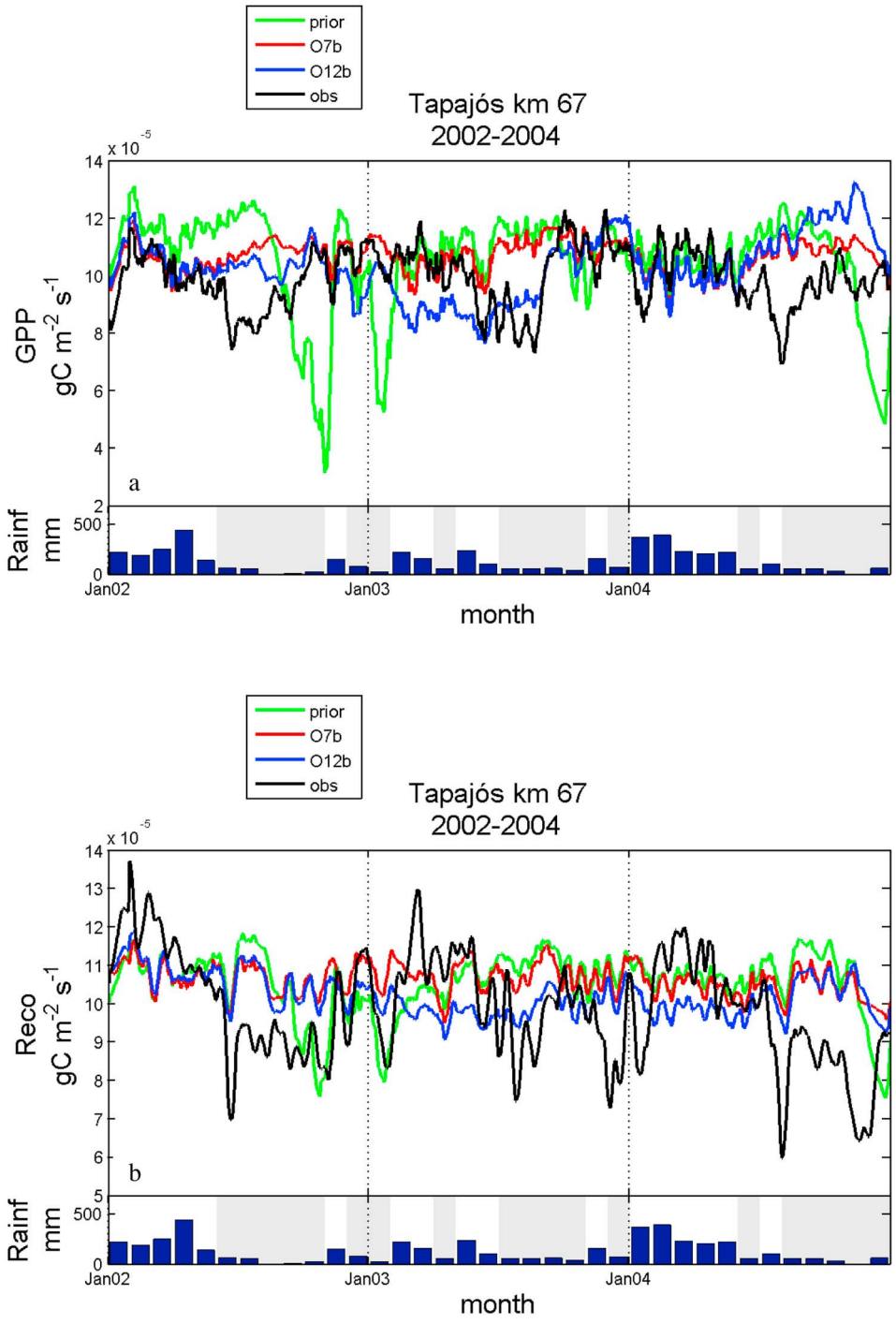

Figure 9. Measured and modeled seasonal patterns of (a) GPP and (b) Reco (g C m^{-2} s^{-1}) (10 day running means): partitioned NEE eddy covariance measurements (black) are compared with the prior model (green), optimization O7b (red), and optimization O12b (blue). The monthly measured precipitation (mm) is shown at the bottom of Figures 9a and 9b. Dry periods are indicated in gray (<100 mm $month^{-1}$).

(by 100 and 200%) in the model, showed only a marginal effect on heterotrophic respiration (not shown). These findings probably show that in this region there is a large soil carbon pool that is relatively passive and decomposes with a very slow turnover rate. Probably the soil carbon dynamics model does not allow enough soil organic matter to transfer from the active to the passive pool to build up enough carbon in the soil over centuries.

4. Conclusions

[43] The prior model showed that the standard ORCHIDEE parameterization behaves like many other global models

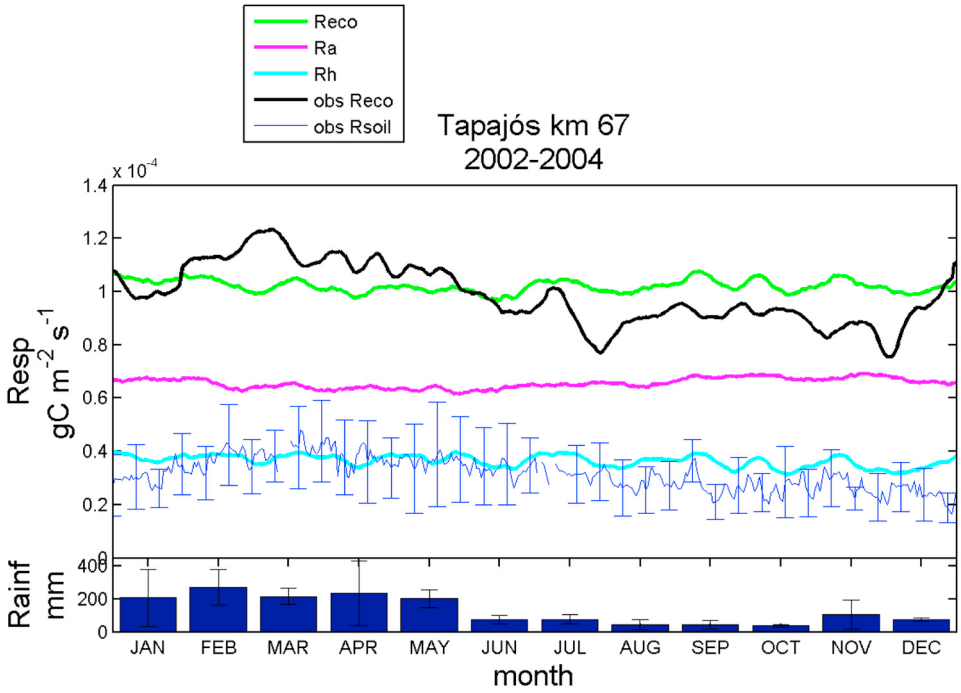

Figure 10. Mean seasonal patterns (2002–2004) of modeled respiration fluxes (g C m^{-2} s^{-1}) based on optimized parameters (O7b): Reco (green), autotrophic respiration Ra (magenta), and heterotrophic respiration (blue). Mean seasonal pattern (2002–2004) of observed Reco derived from eddy covariance measurements (black). Mean season al pattern (April 2001 to April 2003) of observed soil respiration (Rsoil, blue with error bars) from automated soil chambers [*Varner and Keller*, 2009] (April 2001 to April 2003). (top) All lines show 10 day running means. (bottom) The mean seasonal pattern of the monthly measured precipitation (mm).

[*Saleska et al.*, 2003; *Baker et al.*, 2008] and simulates seasonal NEE patterns that are opposite in phase to the eddy flux data at the Tapajós km 67 site. However, optimized scenarios better fitted the observed data. The different optimization scenarios showed that only a few optimized parameters substantially improved the fit with NEE and LE data. Our results confirm in the first place that these forests have the ability to maintain high transpiration and photosynthesis during the dry season and that the soil depth (D_{soil}) and the H_{root} parameter (describing the exponential root profile) are key parameters to model this ability in ORCHIDEE. The resulting values for these parameters are substantially different from the standard values for the tropical evergreen forest PFT. A soil depth of 10 m and a H_{root} parameter of 0.1 are suggested, corresponding to a root distribution that decreases almost linearly with depth and leads to much lower drought stress sensitivity of photosynthesis and transpiration. The retrieved parameter values for Tapajós generally improved the model performance at the Guyaflux and Jaru site. Nevertheless, future work should retrieve and compare optimized model parameters for different evergreen forest sites (with different seasonal NEE patterns) in the Amazon basin in order to study the spatial parameter variability. In addition, redoing optimizations with a multiple-layer soil hydrology [*d'Orgeval et al.*, 2008] may allow better capturing the seasonal drying of the soil from the top, and correlated litter decomposition inhibition in the dry upper soil layers.

[44] Our results indicate that even a higher GPP is reached in the dry season compared to the wet season, most likely caused by a leaf flush at the start of the dry season increasing the photosynthetic capacity of the canopy. The current model structure is not able to simulate such a leaf flush. We therefore suggest improving the ORCHIDEE model by including a specific phenology module that is driven by light availability for the tropical evergreen PFT.

[45] Both the eddy covariance and soil respiration data suggest that there is a drop of ecosystem respiration associated with decreasing soil moisture during the dry season, which was not captured by our modeling results. We suggest a critical evaluation of the respiration parameterization in ORCHIDEE in tropical evergreen sites, taking into account soil water availability as a key driver. To evaluate the simulation of the different respiration components by ORCHIDEE a thorough comparison with multiple data sources is needed. In addition, vertical distribution of soil organic carbon, both its injection by root mortality and its decomposition will be needed. Intuition suggests that the stiffer optimized root distribution should distribute soil C at deeper horizons, where there is enough moisture to sustain decomposition during dry season. A data assimilation exercise with multiple constraints (e.g., partitioned eddy fluxes, soil respiration data, and carbon inventory data) would be appropriate.

[46] In general, we can conclude that our data assimilation exercise resulted in a better view on the underlying factors

Table 4. Initial Carbon Pools of the Tapajós km 67 Site as Simulated by the Spin-Up Runs Compared to Field Measurements From C Inventories (Mg C ha^{-1})[a]

Pool	ORCHIDE		Inventory
	Standard	Optimized	
Aboveground biomass	168.6		145 (±6)[b]
Aboveground necromass	29.3		46 (±5)[b]
Belowground biomass	45.2		17.6 (±6.5)[b]
Leaf biomass	4.71	4.87	6.21 (±0.2)[c]
Total soil C	41.95	50.3	142.1 (±7.1)[d]

[a]The corrected initial biomass of leaf and soil carbon is given based on optimization O12a.
[b]*Saleska et al.* [2003].
[c]*Malhado et al.* [2009].
[d]Value obtained at an oxisol at the Tapajós km 83 site [*Telles et al.*, 2003].

that determine the seasonal patterns of NEE, and leads to important suggestions for model improvement; nevertheless, our results also showed the limitations of flux data assimilation. Several parameters were not identifiable and the risk of overfitting of the model was illustrated. Careful estimation of prior errors of flux data is therefore very important.

[47] Despite of the limitations of our approach, our results show that global vegetation models can be improved substantially by assimilating site level flux data. An improved parameterization of the ORCHIDEE model, particularly soil depth and rooting profiles, based on data assimilation of multiple sites in the Amazon is needed to improve basin-scale simulations and GCM climate projections.

Appendix A

[48] Here only the ORCHIDEE equations that contain parameters that are optimized in this study are briefly listed. The optimized parameters are shown in bold. For a more detailed description of the model, we refer to *Krinner et al.* [2005] and *Santaren et al.* [2007].

A1. Leaf Area

[49] Light decreases in the canopy with increasing LAI following the Lambert-Beer's law [*Monsi and Saeki*, 1953]. The light at the bottom of the canopy (I_l) becomes then:

$$I_l = I_0 \cdot e^{-k \cdot \lambda \cdot LAI} \tag{A1}$$

I_0 is the available light at the top of the canopy, k is the extinction coefficient and λ is a factor describing the leaf clumping. According to *Chen et al.* [2005] this factor is 0.63 for tropical evergreen forest. The actual leaf area is determined by multiplying the leaf biomass from carbon allocation model [*Krinner et al.*, 2005] with the specific leaf area (***SLA***). If the leaf area becomes higher than a PFT-specific prescribed maximum ($\boldsymbol{LAI_{max}}$), than no more carbon will be allocated to leaves.

A2. Photosynthesis

[50] ORCHIDEE uses the *Farquhar et al.* [1980] model. The ratio between the maximum carboxylation capacity (V_{cmax}) and the potential rate of *RuBP* regeneration (V_{jmax}) is assumed to be constant:

$$V_{j\max} = 2 \cdot V_{cmax} \tag{A2}$$

The actual maximum carboxylation capacity ($V_{cmax,actual}$) is depending on leaf age, temperature and soil water limitation according to:

$$V_{c\max,actual} = \varepsilon_{leaf} \cdot \varepsilon_{temp} \cdot \varepsilon_{water} \cdot V_{cmax} \tag{A3}$$

where ε_{leaf} is the leaf efficiency depending on the leaf age, ε_{temp} is the temperature dependency and ε_{water} is the dependency on soil water availability. The relative leaf age of the age class, which is the fraction of the critical leaf age ($\boldsymbol{L_{age}}$) that is reached by that class, is determining the leaf efficiency. When a new leaf class appears its efficiency rises quickly from 0 to 1 by the moment when 3% of the critical age is reached. It stays 1 until a relative age of 50%. After that, the efficiency decreases linearly to 0.3 until the critical leaf age is reached. By convoluting the different leaf age classes the actual V_{cmax} of the entire canopy is calculated. The temperature dependency is determined by a function with a value of 1 at the optimal temperature (T_{opt}) and a value of 0 at the maximum (T_{max}) and minimum temperature (T_{min}):

$$\varepsilon_{temp} = \frac{(T_{air} - T_{\min}) \cdot (T_{air} - T_{\max})}{(T_{air} - T_{\min}) \cdot (T_{air} - T_{\max}) - (T_{air} - T_{opt})^2} \tag{A4}$$

The optimal temperature range for photosynthesis is dynamic and can acclimate to the governing temperature regime according to the following equations:

$$T_{opt} = c_{Topt} + b_{Topt} \cdot T_l + a_{Topt} \cdot T_l^2 \tag{A5}$$

$$T_{\max} = c_{Tmax} + b_{T\max} \cdot T_l + a_{T\max} \cdot T_l^2 \tag{A6}$$

$$T_{\min} = c_{Tmin} + b_{T\min} \cdot T_l + a_{T\min} \cdot T_l^2 \tag{A7}$$

where a_{Ti}, b_{Ti} and c_{Ti} are parameters and T_l is the long-term governing temperature. The dependency (ε_{water}) of V_{cmax} on soil water availability is described by the following response function:

$$\varepsilon_{water} = \frac{2}{1 + \exp(-f_{stress} \cdot f_w)} - 1 \tag{A8}$$

where f_w is the water fraction available for the plant in the root zone (i.e., $f_w = 0$ at wilting point and $f_w = 1$ at field capacity) calculated based on an exponential root profile and the soil depth (D_{soil}):

$$f_w = \max\left(\exp\left(-H_{root} \cdot D_{soil} \cdot a_{deep}\right), \exp\left(-H_{root} \cdot D_{soil} \cdot a_{top}\right)\right) \tag{A9}$$

In equation (A9), H_{root} is a parameter describing the exponential root profile, a_{deep} is the dry fraction of the deep soil

water reservoir and a_{top} is the dry fraction of the topsoil water reservoir. This topsoil reservoir has a variable depth and only exists after rain events. Parameter f_{stress} defines the soil water fraction below which V_{cmax} decreases.

[51] The Farquhar photosynthesis model is used here in combination with the stomatal conductance model according to *Ball et al.* [1987]:

$$g_s = \frac{\beta \cdot A \cdot h_r}{C_a} + g_{offset} \tag{A10}$$

Here β is the slope of the stomatal conductance versus A (the net carbon assimilation rate) linear relationship, h_r the relative humidity (%) and C_a the CO_2 atmospheric concentration.

A3. Autotrophic Respiration

[52] The maintenance respiration (R_m) is a function of temperature (T) and the biomass (B_i) of each pool i [*Ruimy et al.*, 1996]:

$$R_m^i = c(T_i) \cdot B_i \tag{A11}$$

$$c(T_i) = \max\left(c_0^i \cdot (I_{MR} + S_{MR} \cdot T), 0\right) \tag{A12}$$

where I_{MR} and S_{MR} are the coefficients of the linear temperature relationship and c_0 is a parameter specific for each biomass pool i. Growth respiration (R_g) is computed as a constant fraction (K_{GR}) of the assimilates available for growth:

$$R_g = K_{GR} \cdot (A - R_m) \tag{A13}$$

A4. Heterotrophic Respiration

[53] Two litter pools (metabolic and structural) and three soil organic matter pools of increasing turnover are considered in the model. The heterotrophic respiration in each carbon pool is governed by a first-order linear differential equation, where pool specific turnovers have soil moisture and soil temperature dependencies.

$$R_h = \sum_s \alpha_s \cdot B_s \cdot c_H \cdot c_T \tag{A14}$$

B_s is the size of each soil carbon pool, α_s is a pool specific coefficient partitioning heterotrophic respiration into pools, c_T and c_H are inhibition factors that represent the slowing down of decomposer activity at low temperatures or in dry (or too wet) soil. The soil/litter humidity inhibition factor c_H is:

$$c_H = \max\left(c_{H\min}, \min\left(1, aH^2 + bH + c\right)\right) \tag{A15}$$

where H is humidity of the litter or the organic soil layer. The particular optimal form of c_H depends strongly on the assumptions and formulation of the hydrological scheme used. Exploration of the c_H function resulted the choice to set a constant value of 1 for a, 0.25 for c_{Hmin} and to vary b (0–10) and c (0–1) to get realistic shapes of the c_H function. H is calculated as follows:

$$H_{litter} = \exp\left(\frac{-h_{wet}}{h_{crit}}\right) \tag{A16}$$

$$H_{soil,i} = hum_i \cdot \left(\exp\left(\frac{-Z_{soil,i-1}}{Z_{decomp}}\right) - \exp\left(\frac{-Z_{soil,i}}{Z_{decomp}}\right)\right) \tag{A17}$$

where h_{wet} is the height of the wet litter, h_{crit} is the total height of the litter layer, hum_i is the soil water content in layer i, $Z_{soil,i}$ the depth of soil layer i and Z_{decomp} the parameter describing the exponential decomposition profile. The temperature inhibition factor c_T for heterotrophic respiration (in litter and soil) is a Q_{10} function of soil temperature (T_{soil}).

$$c_T = \min\left(1, \exp\left(\ln(Q_{10}) \cdot \frac{T_{soil} - 30}{10}\right)\right) \tag{A18}$$

[54] **Acknowledgments.** The authors would like to thank Diego Santaren for his contribution to the development of the optimization code, François Delage and Peter Rayner for the contribution to the development of the tangent linear model, and two anonymous reviewers for their useful comments to a previous version of the manuscript. We are grateful to L. Hutyra, S. Saleska, and S. Wofsy for making the eddy flux data of the Tapajós km 67 site available at the Oak Ridge National Laboratory Distributed Active Archive Center, Celso von Randow and Antonio O. Manzi for providing the Reserva Jaru data, and Benoit Burban for the Guyaflux data.

References

Akaike, H. (1974), A new look at the statistical model identification: System identification and time-series analysis, *IEEE Trans. Autom. Control*, *19*, 716–723, doi:10.1109/TAC.1974.1100705.

Baker, I. T., L. Prihodko, A. S. Denning, M. Goulden, S. Miller, and H. R. da Rocha (2008), Seasonal drought stress in the Amazon: Reconciling models and observations, *J. Geophys. Res.*, *113*, G00B01, doi:10.1029/2007JG000644.

Ball, J. T., I. E. Woodrow, and J. A. Berry (1987), A model predicting stomatal conductance and its contribution to the control of photosynthesis under different environmental conditions, in *Progress in Photosynthesis Research*, vol. 4, edited by I. Biggins, pp. 221–224, Martinus Nijhoff, Dordrecht, Netherlands.

Bonal, D., et al. (2008), The impact of severe dry season on net ecosystem exchange in the Neotropical rainforest of French Guiana, *Global Change Biol.*, *14*, 1–17, doi:10.1111/j.1365-2486.2008.01610.x.

Botta, A., N. Viovy, P. Ciais, P. Friedlingstein, and P. Monfray (2000), A global prognostic scheme of leaf onset using satellite data, *Global Change Biol.*, *6*(7), 709–725, doi:10.1046/j.1365-2486.2000.00362.x.

Bousquet, P., P. Peylin, P. Ciais, C. Le Quere, P. Friedlingstein, and P. P. Tans (2000), Regional changes in carbon dioxide fluxes of land and oceans since 1980, *Science*, *290*(5495), 1342–1346, doi:10.1126/science.290.5495.1342.

Braswell, B. H., W. J. Sacks, E. Linder, and D. S. Schimel (2005), Estimating diurnal to annual ecosystem parameters by synthesis of a carbon flux model with eddy covariance net ecosystem exchange observations, *Global Change Biol.*, *11*, 335–355, doi:10.1111/j.1365-2486.2005.00897.x.

Carvalhais, N., et al. (2008), Implications of the carbon cycle steady state assumption for biogeochemical modeling performance and inverse parameter retrieval, *Global Biogeochem. Cycles*, *22*, GB2007, doi:10.1029/2007GB003033.

Carvalhais, N., M. Reichstein, P. Ciais, G. J. Collatz, M. D. Mahecha, L. Montangnani, D. Papale, S. Rambal, and J. Seixas (2010), Identification of vegetation and soil carbon pools out of equilibrium in a process model via eddy covariance and biometric constraints, *Global Change Biol.*, doi:10.1111/j.1365-2486.2010.02173.x.

Chen, J. M., C. H. Menges, and S. G. Leblanc (2005), Global mapping of foliage clumping index using multi-angular satellite data, *Remote Sens. Environ.*, *97*(4), 447–457, doi:10.1016/j.rse.2005.05.003.

Chevallier, F., N. Viovy, M. Reichstein, and P. Ciais (2006), On the assignment of prior error in Bayesian inversions of CO_2 surface fluxes, *Geophys. Res. Lett.*, *33*, L13802, doi:10.1029/2006GL026496.

Cox, P., R. A. Betts, M. Collins, P. P. Harris, C. Huntingford, and C. D. Jones (2004), Amazonian forest dieback under climate-carbon cycle projections for the 21st century, *Theor. Appl. Climatol.*, *78*, 137–156, doi:10.1007/s00704-004-0049-4.

Domingues, T. F., J. A. Berry, L. A. Martinelli, J. Ometto, and J. R. Ehleringer (2005), Parameterization of canopy structure and leaf-level gas exchange for an eastern Amazonian tropical rain forest (Tapajos National Forest, Para, Brazil), *Earth Interact.*, *9*(17), 1–23, doi:10.1175/EI149.1.

d'Orgeval, T., J. Polcher, and P. de Rosnay (2008), Sensitivity of the West African hydrological cycle in ORCHIDEE to infiltration processes, *Hydrol. Earth Syst. Sci.*, *12*(6), 1387–1401, doi:10.5194/hess-12-1387-2008.

Ducoudré, N. I., K. Laval, and A. Perrier (1993), SECHIBA, a new set of parameterizations of the hydrologic exchanges at the land-atmosphere interface within the LMD atmospheric general circulation model, *J. Clim.*, *6*, 248–273, doi:10.1175/1520-0442(1993)006<0248:SANSOP>2.0.CO;2.

Farquhar, G. D., S. von Caemmerer, and J. A. Berry (1980), A biochemical model of photosynthetic CO_2 assimilation in leaves of C_3 species, *Planta*, *149*, 78–90, doi:10.1007/BF00386231.

Field, C. B., M. J. Behrenfeld, J. T. Randerson, and P. Falkowski (1998), Primary production of the biosphere: Integrating terrestrial and oceanic components, *Science*, *281*(5374), 237–240, doi:10.1126/science.281.5374.237.

Grant, R. F., L. R. Hutyra, R. C. Oliveira, J. W. Munger, S. R. Saleska, and S. C. Wofsy (2009), Modeling the carbon balance of Amazonian rain forests: Resolving ecological controls on net ecosystem productivity, *Ecol. Monogr.*, *79*(3), 445–463, doi:10.1890/08-0074.1.

Huete, A. R., K. Didan, Y. E. Shimabukuro, P. Ratana, S. R. Saleska, L. R. Hutyra, W. Yang, R. R. Nemani, and R. Myneni (2006), Amazon rainforests green-up with sunlight in dry season, *Geophys. Res. Lett.*, *33*, L06405, doi:10.1029/2005GL025583.

Hutyra, L. R., J. W. Munger, S. R. Saleska, E. Gottlieb, B. C. Daube, A. L. Dunn, D. F. Amaral, P. B. de Camargo, and S. C. Wofsy (2007), Seasonal controls on the exchange of carbon and water in an Amazonian rain forest, *J. Geophys. Res.*, *112*, G03008, doi:10.1029/2006JG000365.

Hutyra, L., S. Wofsy, and S. Saleska (2008), LBA-ECO CD-10 CO_2 and H_2O eddy fluxes at km 67 Tower Site, Tapajos National Forest, doi:10.3334/ORNLDAAC/860, Distributed Active Arch. Cent., Oak Ridge Natl. Lab., Oak Ridge, Tenn. (Available at http://www.daac.ornl.gov)

Ichii, K., H. Hashimoto, M. A. White, C. Potter, L. R. Hutyra, A. R. Huete, R. B. Myneni, and R. R. Nemani (2007), Constraining rooting depths in tropical rainforests using satellite data and ecosystem modeling for accurate simulation of gross primary production seasonality, *Global Change Biol.*, *13*(1), 67–77, doi:10.1111/j.1365-2486.2006.01277.x.

Kattge, J., W. Knorr, T. Raddatz, and C. Wirth (2009), Quantifying photosynthetic capacity and its relationship to leaf nitrogen content for global-scale terrestrial biosphere models, *Global Change Biol.*, *15*(4), 976–991, doi:10.1111/j.1365-2486.2008.01744.x.

Kleidon, A., and M. Heimann (1999), Deep-rooted vegetation, Amazonian deforestation, and climate: Results from a modelling study, GCTE/LUCC Research Letter, *Glob. Ecol. Biogeogr.*, *8*(5), 397–405, doi:10.1046/j.1365-2699.1999.00150.x.

Krinner, G., N. Viovy, N. de Noblet-Ducoudré, J. Ogée, J. Polcher, P. Friedlingstein, P. Ciais, S. Sitch, and I. C. Prentice (2005), A dynamic global vegetation model for studies of the coupled atmosphere-biosphere system, *Global Biogeochem. Cycles*, *19*, GB1015, doi:10.1029/2003GB002199.

Kruijt, B., J. A. Elbers, C. von Randow, A. C. Araújo, P. J. Oliveira, A. Culf, A. O. Manzi, A. D. Nobre, P. Kabat, and E. J. Moors (2004), The robustness of eddy correlation fluxes for Amazon rain forest conditions, *Ecol. Appl.*, *14*, 101–113, doi:10.1890/02-6004.

Lasslop, G., M. Reichstein, J. Kattge, and D. Papale (2008), Influences of observation errors in eddy flux data on inverse model parameter estimation, *Biogeosciences*, *5*, 1311–1324, doi:10.5194/bg-5-1311-2008.

Luyssaert, S., et al. (2007), CO_2 balance of boreal, temperate, and tropical forests derived from a global database, *Global Change Biol.*, *13*(12), 2509–2537, doi:10.1111/j.1365-2486.2007.01439.x.

Malhado, A. C. M., M. H. Costa, F. Z. de Lima, K. C. Portilho, and D. N. Figueiredo (2009), Seasonal leaf dynamics in an Amazonian tropical forest, *For. Ecol. Manage.*, *258*(7), 1161–1165, doi:10.1016/j.foreco.2009.06.002.

Malhi, Y., J. T. Roberts, R. A. Betts, T. J. Killeen, W. Li, and C. A. Nobre (2008), Climate change, deforestation, and the fate of the Amazon, *Science*, *319*(5860), 169–172, doi:10.1126/science.1146961.

Markewitz, D., S. Devine, E. A. Davidson, P. Brando, and D. C. Nepstad (2010), Soil moisture depletion under simulated drought in the Amazon: Impacts on deep root uptake, *New Phytol.*, *187*(3), 592–607, doi:10.1111/j.1469-8137.2010.03391.x.

Misra, V. (2008), Coupled air, sea, and land interactions of the South American monsoon, *J. Clim.*, *21*(23), 6389–6403, doi:10.1175/2008JCLI2497.1.

Moffat, A. M., et al. (2007), Comprehensive comparison of gap-filling techniques for eddy covariance net carbon fluxes, *Agric. For. Meteorol.*, *147*(3–4), 209, doi:10.1016/j.agrformet.2007.08.011.

Monsi, M., and T. Saeki (1953), Über den Lichtfaktor in den Pflanzengesellschaften unde seine Bedeutung für die Stoffproduktion, *Jpn. J. Bot.*, *14*, 22–52.

Myneni, R. B., et al. (2007), Large seasonal swings in leaf area of Amazon rainforests, *Proc. Natl. Acad. Sci. U. S. A.*, *104*, 4820–4823, doi:10.1073/pnas.0611338104.

Nepstad, D. C., C. R. Decarvalho, E. A. Davidson, P. H. Jipp, P. A. Lefebvre, G. H. Negreiros, E. D. Dasilva, T. A. Stone, S. E. Trumbore, and S. Vieira (1994), The role of deep roots in the hydrological and carbon cycles of Amazonian forests and pastures, *Nature*, *372*(6507), 666–669, doi:10.1038/372666a0.

Nepstad, D., et al. (2002), The effects of partial throughfall exclusion on canopy processes, aboveground production, and biogeochemistry of an Amazon forest, *J. Geophys. Res.*, *107*(D20), 8085, doi:10.1029/2001JD000360.

Oliveira, R., T. Dawson, S. Burgess, and D. Nepstad (2005), Hydraulic redistribution in three Amazonian trees, *Oecologia*, *145*(3), 354–363, doi:10.1007/s00442-005-0108-2.

Papale, D., et al. (2006), Towards a standardized processing of net ecosystem exchange measured with eddy covariance technique: Algorithms and uncertainty estimation, *Biogeosciences*, *3*, 571–583, doi:10.5194/bg-3-571-2006.

Parton, W., J. Stewart, and C. Cole (1988), Dynamics of C, N, P, and S in grassland soil: A model, *Biogeochemistry*, *5*, 109–131, doi:10.1007/BF02180320.

Piao, S., S. Luyssaert, P. Ciais, I. A. Janssens, A. Chen, C. Cao, J. Fang, P. Friedlingstein, Y. Luo, and S. Wang (2010), Forest annual carbon cost: A global-scale analysis of autotrophic respiration, *Ecology*, *91*(3), 652–661, doi:10.1890/08-2176.1.

Poulter, B., U. Heyder, and W. Cramer (2009), Modeling the sensitivity of the seasonal cycle of GPP to dynamic LAI and soil depths in tropical rainforests, *Ecosystems*, *12*, 517–533, doi:10.1007/s10021-009-9238-4.

Reichstein, M., et al. (2005), On the separation of net ecosystem exchange into assimilation and ecosystem respiration: Review and improved algorithm, *Global Change Biol.*, *11*, 1424–1439, doi:10.1111/j.1365-2486.2005.001002.x.

Rice, A. H., E. P. Hammond, S. R. Saleska, L. Hutyra, M. Palace, M. Keller, P. B. de Carmargo, K. Portilho, D. Marques, and S. C. Wofsy (2008), LBA-ECO CD-10 forest litter data for km 67 Tower Site, Tapajos National Forest, doi:10.3334/ORNLDAAC/862, Distributed Active Arch. Cent., Oak Ridge Natl. Lab., Oak Ridge, Tenn. (Available at http://www.daac.ornl.gov)

Richardson, A. D., D. Y. Hollinger, G. G. Burba, K. J. Davis, L. B. Flanagan, G. G. Katul, J. William Munger, D. M. Ricciuto, P. C. Stoy, and A. E. Suyker (2006), A multi-site analysis of random error in tower-based measurements of carbon and energy fluxes, *Agric. For. Meteorol.*, *136*(1–2), 1–18, doi:10.1016/j.agrformet.2006.01.007.

Romero-Saltos, H., L. S. L. Sternberg, M. Z. Moreira, and D. C. Nepstad (2005), Rainfall exclusion in an eastern Amazonian forest alters soil water movement and depth of water uptake, *Am. J. Bot.*, *92*, 443–455, doi:10.3732/ajb.92.3.443.

Ruimy, A., L. Kergoat, C. B. Field, and B. Saugier (1996), The use of CO_2 flux measurements in models of the global terrestrial carbon budget, *Global Change Biol.*, *2*, 287–296, doi:10.1111/j.1365-2486.1996.tb00080.x.

Saleska, S. R., et al. (2003), Carbon in Amazon forests: Unexpected seasonal fluxes and disturbance-induced losses, *Science*, *302*, 1554–1557, doi:10.1126/science.1091165.

Santaren, D., P. Peylin, N. Viovy, and P. Ciais (2007), Optimizing a process-based ecosystem model with eddy-covariance flux measurements: A pine forest in southern France, *Global Biogeochem. Cycles*, *21*, GB2013, doi:10.1029/2006GB002834.

Sellers, P. J., et al. (1997), Modeling the exchanges of energy, water, and carbon between continents and the atmosphere, *Science*, *275*(5299), 502–509, doi:10.1126/science.275.5299.502.

Sitch, S., et al. (2003), Evaluation of ecosystem dynamics, plant geography and terrestrial carbon cycling in the LPJ dynamic global vegetation model, *Global Change Biol.*, *9*(2), 161–185, doi:10.1046/j.1365-2486.2003.00569.x.

Tarantola, A. (1987), *Inverse Problem Theory: Methods for Data Fitting and Parameter Estimation*, Elsevier, Amsterdam.

Taylor, K. E. (2001), Summarizing multiple aspects of model performance in a single diagram, *J. Geophys. Res.*, *106*, 7183–7192, doi:10.1029/2000JD900719.

Telles, E. C. C., P. B. de Camargo, L. A. Martinelli, S. E. Trumbore, E. S. da Costa, J. Santos, N. Higuchi, and R. C. Oliveira (2003), Influence of soil texture on carbon dynamics and storage potential in tropical forest soils of Amazonia, *Global Biogeochem. Cycles*, *17*(2), 1040, doi:10.1029/2002GB001953.

ter Steege, H., et al. (2006), Continental-scale patterns of canopy tree composition and function across Amazonia, *Nature*, *443*, 444–447, doi:10.1038/nature05134.

Varner, R. K., and M. M. Keller (2009), LBA-ECO TG-07 soil CO_2 flux by automated chamber, Para, Brazil: 2001–2003, doi:10.3334/ORNLDAAC/927, Distributed Active Arch. Cent., Oak Ridge Natl. Lab., Oak Ridge, Tenn. (Available at http://daac.ornl.gov)

von Randow, C., et al. (2004), Comparative measurements and seasonal variations in energy and carbon exchange over forest and pasture in South West Amazonia, *Theor. Appl. Climatol.*, *78*(1), 5–26, doi:10.1007/s00704-004-0041-z.

Williams, M., et al. (2009), Improving land surface models with FLUXNET data, *Biogeosciences*, *6*(7), 1341–1359, doi:10.5194/bg-6-1341-2009.

Zhu, C., R. H. Byrd, P. Lu, and J. Nocedal (1995), A limited memory algorithm for bound constrained optimization, *SIAM J. Sci. Stat. Comput.*, *16*(5), 1190–1208, doi:10.1137/0916069.

C. Bacour, NOVELTIS, Parc Technologique du Canal 2, avenue de l'Europe, F-31520 Ramonville-Saint-Agne, France.

D. Bonal, INRA Nancy, UMR INRA-UHP 1137 "Ecologie et Ecophysiologie Forestière," F-54280 Champenoux, France.

P. Ciais, Laboratory of Climate Sciences and the Environment, Joint Unit of CEA-CNRS, L'Orme des Merisiers, F-91191 Gif-sur-Yvette, France.

P. Peylin, Laboratory of Biogéochimie et Ecologie des Milieux Continentaux, F-78850 Thiverval-Grignon, France.

K. Steppe and H. Verbeeck, Laboratory of Plant Ecology, Department of Applied Ecology and Environmental Biology, Faculty of Bioscience Engineering, Ghent University, Coupure Links 653, B-9000 Ghent, Belgium. (hans.verbeeck@ugent.be)